POLITECNICO MILANO 1863

SCUOLA DI INGEGNERIA INDUSTRIALE E DELL'INFORMAZIONE

EXECUTIVE SUMMARY OF THE THESIS

PEMFC catalyst layer degradation - an experimental study of voltage limits effect in realistic cycling to develop a platinum dissolution model

TESI MAGISTRALE IN ENERGY ENGINEERING – INGEGNERIA ENGINEERING

AUTHOR: CHIARA ARTINI

ADVISOR: Prof. ANDREA BARICCI

ACADEMIC YEAR: 2020-2021

1. Introduction

PEMFCs are a promising technology to decarbonize the automotive sector, thanks to their zero CO_2 emissions. Nonetheless, they still present important costs and durability issues, due to the expenditure and to the rapid ageing of some components. Among the components, the Catalyst Layer (CL), together with the membrane, is the most critical one. It is composed of platinum nanoparticles, a carbon porous structure and ionomer. In normal PEMFCs operating conditions platinum shows an electrochemical unstable behavior and can dissolve in the ionomer, leading to a reduction of the ElectroChemically active Surface Area (ECSA).

Many experimental studies have been done to understand the effect of voltage cycling and operating conditions on CL degradation[1], and several platinum dissolution models with different level of complexity have been developed to simulate this phenomenon and achieve a deeper comprehension of its physics [2][3]. It is worth underlining that in the literature there is not an overall consensus about different reactions and mechanisms leading to platinum dissolution.

The goal of this work is to investigate CL degradation during voltage cycling, focusing on the effect of different potential values and profiles. To this aim, a simple physics-based platinum dissolution model was developed, and an experimental analysis was made, performing different Accelerated Stress Tests (ASTs). The model was then used to reproduce the experimental results and to explain the observed phenomena.

2. Model description

The proposed model aims to simulate platinum dissolution given different voltage profiles and operating conditions. It was developed starting from the work of Schneider et al.[2]. Here it is an outline of the main hypothesis:

-The model is zero-dimensional. Although the potential, and consequently the other described quantities are not uniform across the CL, such a model can provide quite an accurate description, reducing complexity and computational times.

-The Particle Radius Distribution (PRD) is approximated as lognormal and discretized with a finite number of spherical particle groups, characterized by the radius r_i and the particle number n_i. All particles of the same group undergo the same transition: they either shrink or grow, and they cannot move to other groups. During the degradation, if the radius of one group decreases under a minimum value, the group is eliminated and the correspondent amount of platinum is considered as dissolved in the ionomer.

-Reactions which take place at potentials higher than 0.95 V (i.e. carbon corrosion) are neglected. Indeed the model is built to run in a potential range corresponding to normal operating conditions.

During normal automotive operation, when the cathode potential range between 0.6 V and 0.95 V, platinum can dissolve and redeposit according to reaction (1), called anodic dissolution.

$$Pt \rightleftarrows Pt^{2+} + 2e^- \qquad [\Phi_{diss}^{ref} = 1.188\ V] \qquad (1)$$

$$r_{Adiss}^{i} = k_{Ad}(1-\theta_{PtO}^{i})\left[\exp\left(\frac{\alpha_{a1} n_1 F}{RT}(\Phi - \Phi_{Ad}^{i})\right) - \left(\frac{c_{Pt^{2+}}}{c_{Pt^{2+},ref}}\right)\exp\left(-\frac{\alpha_{c1} n_1 F}{RT}(\Phi - \Phi_{Ad}^{i})\right)\right] \qquad (2)$$

The reaction rate is modelled with a Butler-Volmer equation ((2)). It thus depends on the difference between the imposed potential and the equilibrium potential, shifted from the reference value by means of a Gibbs-Thompson correction to account for the particle size effect. Hence, particles with different radius have a different equilibrium potential and a different dissolution reaction rate. Smaller particles are more prone to dissolution while Pt redeposition mainly takes place on bigger particles. During the lifecycle, smaller particles will therefore shrink and eventually disappear, while bigger particles will grow, leading to an increase of the mean particle radius, a reduction of ECSA (inversely proportional to the radius) and a decay of performances. This mechanism is known as Ostwald ripening.

Both the forward and the backward reaction are hindered by the presence of Pt oxides. Oxidation can also take place (reaction (3)), preventing platinum from dissolving but also temporarily reducing its active area.

$$Pt + H_2O \rightleftarrows PtO + 2H^+ + 2e^- \qquad [\Phi_{ox}^{ref} = 0.98\ V] \qquad (3)$$

$$r_{Ox} = k_{ox}\left[(1-\theta_{PtO}) * \exp\left(-\frac{\omega_{PtO}\theta_{PtO}}{RT}\right)\exp\left(\frac{\alpha_{a2} n_{OxR} F}{RT}(\Phi - \Phi_{ox})\right) - \theta_{PtO} a_{H^+}^2 \exp\left(-\frac{\alpha_{c2} n_{OxR} F}{RT}(\Phi - \Phi_{ox})\right)\right] \qquad (4)$$

The oxidation reaction rate also follows the Butler-Volmer equation, modified with an exponential term to reproduce the experimentally observed logarithmic oxide growth [3]. The equilibrium potential includes the particle size effect, resulting in different reactions rates and different oxide coverage for different particle groups.

When the platinum is oxidized, it can either reduce according to the backward oxidation reaction, or chemically dissolve directly in the electrolyte, according to reaction (5), which is independent on potential and then modelled with a chemical reaction rate (equation (6)).

$$PtO + 2H^+ \rightleftarrows Pt^{2+} + H_2O \qquad (5)$$

$$r_{chem} = k_{chem}\theta_{PtO} c_{H^+}^2 \qquad (6)$$

Another loss source is platinum migration into the membrane. As Pt dissolves in the electrolyte, a concentration gradient is established, which enhances Pt migration toward the membrane and its eventual precipitation, resulting from reaction with crossover hydrogen. This behaviour is modelled as a diffusive flux. After the precipitation platinum is not active anymore.

Material balances are then necessary to complete the model, describing the time variation of oxide coverage, Pt concentration, and particle radius, whose derivative depends on reaction rates previously described. As oxide coverage and particle radius are different for each particles group, 2N+1 material balances are required, where N is the groups number.

The model is implemented with Matlab, and the differential equations system is solved with the ODE solver *ode15s* with variable time steps.

Oxidation and anodic dissolution parameters were calibrated with experimental data, while other parameters were taken from ref [2].

Some specific tests were performed to investigate oxide formation: Cyclic Voltammetries (CV) with different Upper Potential Limits (UPL) and Scan Rates, and Holding Linear Sweep Voltammetries (LSV), with different UPLs and holding times. In holding LSVs the potential was kept constant at a certain UPL for a certain holding time and then decreased linearly while detecting the current. The oxide coverage formed during the holding period was measured by integrating the current. Oxidation parameters were calibrated to reproduce the oxide reduction peak potential measured in CVs and the oxide coverage measured in holding-LSVs (Figure 1).

Anodic dissolution parameters were calibrated on electrocatalyst AST experimental data taken from another thesis work[4]. The base cycle of this standard AST (defined by the US D.o.E [5]) is a voltage square wave between 0.6 V and 0.95 V, with a dwell time of 3 s and a rise time of 0.5 s. The anodic dissolution parameters were varied to reproduce the ECSA loss experimental trend

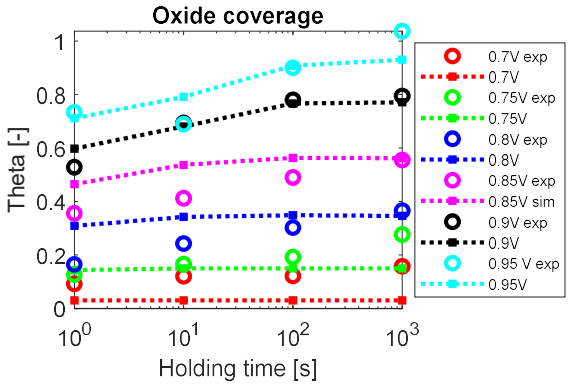

Figure 1 - Holding LSVs oxide coverage: experimental vs simulated results (dashed lines)

(Figure 2). The parameters set resulting from this calibration will be referred to as SET 0. For a more detailed description of the model and of the calibration please refer to chapter 3.

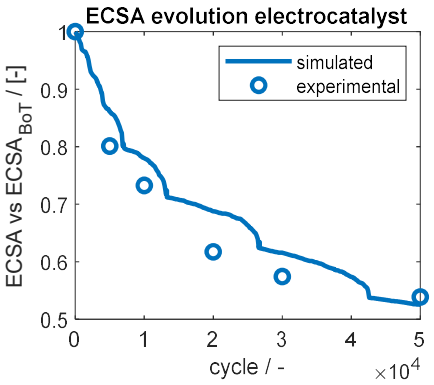

Figure 2 - ECSA evolution - D.o.E AST electrocatalyst

3. Experimental

Methodology

Experimental procedures were performed using a Multi Zero-gradient hardware, allowing to test 4 different cells at the same time. The flow field is indeed divided in four electrically insulated parts, and each sample has separate current collectors. Therefore, each sample operates as if it is in a standard single cell hardware. The cell area is small and the used flowrates are much higher than stoichiometric ones. Hence, gas relative humidity and oxygen concentration in the channel are kept almost constant among the different samples. The same catalyst coated membrane was employed for all the tests.

Several ASTs with different potential profiles were performed. Characterization tests were executed at the Beginning of Test (BoT) and repeated at each stop of the AST. Among them the most important for this analysis were: Cyclic Voltammetries (CVs) to measure the ECSA, Linear Sweep Voltammetries (LSVs) to measure the hydrogen crossover and the membrane electric resistance, polarization curves to monitor cell performances.

Ageing protocols were designed to investigate catalyst degradation mechanisms. The initial reference was the Low Power AST designed in the frame of the European H2020 ID-FAST project [6], which aims at reproducing the degradation of realistic automotive low power operation. All the ASTs were performed with hydrogen/air feeding and an operating temperature of 71°C. Each AST was performed simultaneously on different samples thanks to the Multi-0G hardware. The shape of the potential profile, which characterizes the AST, is the same for all the samples, while the imposed potential values are different.

AST design and experimental results

IDFAST Low Power AST is designed in galvanostatic mode and performed with a 70/60% (anode/cathode) relative humidity. The base profile is a square wave ranging between the current values which correspond to 0.85 V and 0.7 V at BoT, with dwell time of 30 s and 12 s respectively. These two steps are repeated for 6 times and at the end of each AST cycle a short stop of 110 s at nearly 0 V is introduced, realized with the interruption of the air feeding. The results of this AST were taken from ref [4]. Starting from this protocol, several degradation tests have been designed. An overview of the ASTs design and of the obtained results is shown in Figure 4.

The effect of the voltage regulation and of the Upper Potential Limit (UPL) was investigated with AST 1. This test is a variation of the IDFAST Low Power AST: potential was imposed instead of current and different UPLs were used for different samples (0.85 V for sample 1 and 0.9 V for sample 2). The Lower Potential Limit (LPL) was set to 0.7 V (Figure 3). Looking at the ECSA trends (Figure 5) some remarks can be made:

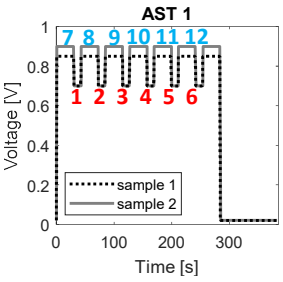

Figure 3 - AST 1 base cycle

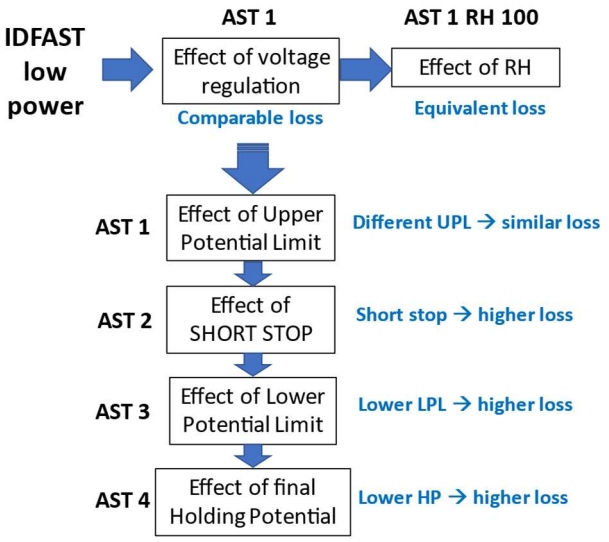

Figure 4 - Overview of accelerated stress tests: design and results

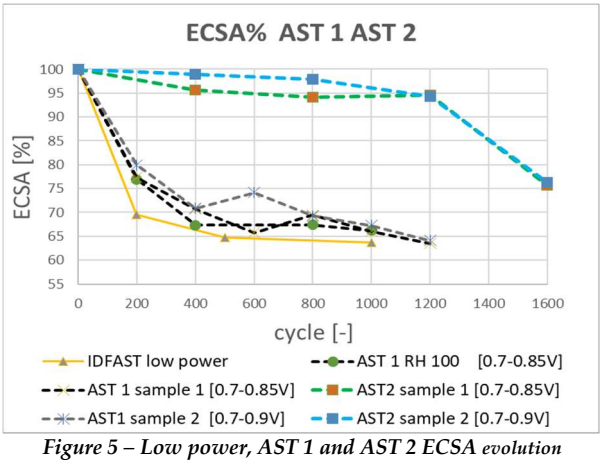

Figure 5 – Low power, AST 1 and AST 2 ECSA evolution

-the ECSA shows a rapid and considerable decrease: it drops below 80% of the initial value in the first 200 cycles for both samples, and then stabilizes around 65%;

- IDFAST low power and AST 1 sample 1, which only differ in regulation, show quite similar ECSA trends, with a difference of 5-7%: the potentiostatic mode did not results in a significative difference in degradation;

-AST 1 samples 1 and 2 have similar ECSA trends: a higher UPL did not cause a higher degradation, differently from the general knowledge available in the literature [1].

Current was also measured during the test execution, and its profile in two subsequent cycles is shown in Figure 6. There is a significative current reduction among subsequent steps at the same voltage, but after the short stop the performance loss is immediately recovered. This can be ascribed to the formation of a Pt oxide which is not completely reduced at 0.7 V and therefore grows during the cycle, while it is strongly reduced going to 0 V, allowing the performance recover. After many cycles a current reduction among different AST cycles can be observed, which can be attributed not only to an increasing oxide coverage but mainly to an irreversible performance decay. The effect of relative humidity was then investigated by repeating AST 1 in totally humified conditions. An equivalent ECSA trend was obtained (Figure 5), suggesting a negligible impact of RH on degradation.

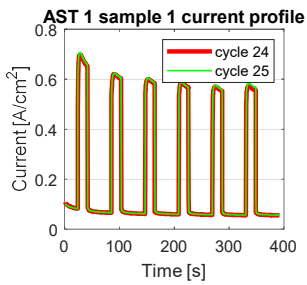

Figure 6 - AST 1 sample 1 current profiles

AST 2 was designed to investigate the ageing effect of short stops. To this aim the same potential profile of AST 1 was used, without the short stops for the first 1200 cycles, and with short stops in the last 400 cycles. The AST was performed on two samples with the same UPLs and LPLs used for AST 1.

A really limited ECSA loss (Figure 5) is observed up to 1200 cycles, while a significant decrease is measured in the last 400 cycles, meaning that short stops have a much stronger effect on degradation with respect to the cycling only. As observed for AST 1 the two samples show a similar ECSA trend: the higher UPL did not impact significantly on the degradation, even without the short stop effect.

Current values of low voltage steps detected during the test are plotted in Figure 7 (steps number are defined in Figure 3). In the first 1200 cycles (before the red line) a progressive performance loss can be observed, which is almost completely recovered every 200 cycles when a stop is introduced. This trend can be again explained with the formation of an oxide that keeps growing during subsequent cycles and is reduced only with the short stop.

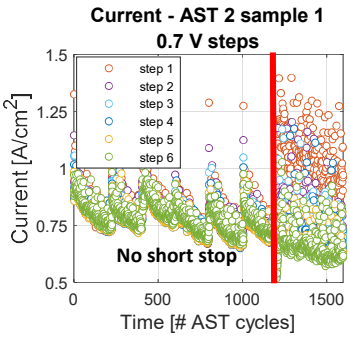

Figure 7 – Current -AST 2 sample 1 low voltage steps

AST 3 and AST 4 were designed to understand the effect of the minimum potential. AST 3 base voltage profile (Figure 8) is a square wave continuously cycling between the UPL (set to 0.85 V for all the samples) and the LPL, set to 0.7 V, 0.6 V and 0.4 V respectively for sample 1, 2 and 3.

AST 4 base cycle is composed with a cycling part ranging between 0.7 and 0.85 V followed by a final holding at different Holding Potential (HP) values: 0.7 V, 0.6 V, 0.4 V and 0.2 V respectively for sample

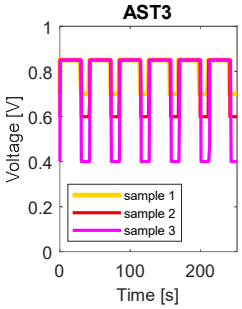

Figure 8 - AST 3 base cycle

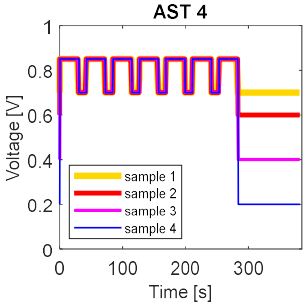

Figure 9 - AST 4 base cycle

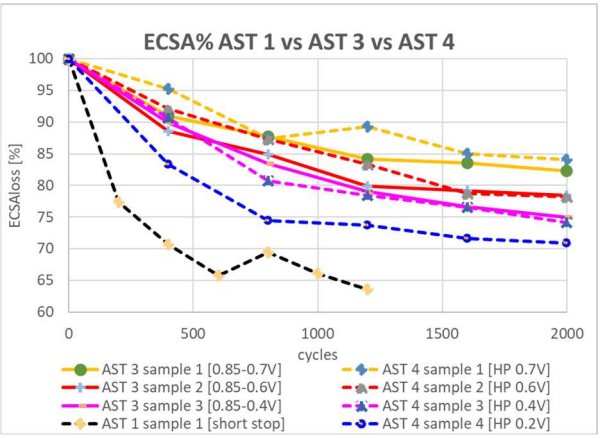

Figure 10 - ECSA evolution: AST 1, AST 3, AST 4

1, 2, 3 and 4 (Figure 9). Both AST 3 and AST 4 ECSA trends show an increasing loss (Figure 10) for the samples reaching lower potential values. It thus emerged that lower minimum potentials lead to stronger degradation, both when the potential is continuously reduced under 0.7 V, as in AST3, and when it is only periodically reduced under this value at the end of each AST cycle, as in AST 4. It is also worth noting that sample 4 shows a lower ECSA loss with respect to AST 1 results, meaning that reducing the potential down to 0.2V does not have the same degrading effect of the short stop. AST 4 current detected during low voltage steps show increasing current values from sample 1 to sample 4 (mean values are reported in Table 1), although the potential is the same (0.7 V). This can be again explained with the formation of an oxide which grows during the cycling and is differently reduced in the four samples: lower holding values enhance the oxide reduction, resulting in a boosted performance.

Sample	1	2	3	4
Mean current [A]	0.3075	0.4207	0.4682	0.5122

Table 1 - AST 4 current mean values of low voltage [0.7V] steps

Moreover, the current plot of the high voltage steps (Figure 11) show a reversible performance decrease which is recovered every 200 cycles when a short stop is introduced. This suggests that the oxide is not completely reduced, even going down to 0.4 V. This is a really interesting result, as this potential value is lower than the one typically considered in the literature for the reduction of PtO, which is around 0.6 V [2][7]. A possible interpretation of this phenomenon is the presence of a more resistant oxide. For more details about experimental results please refer to chapter 4.

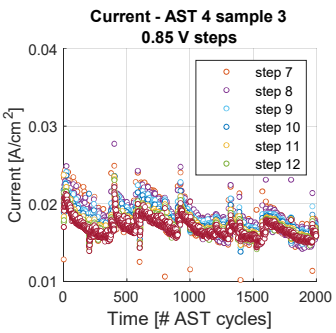

Figure 11 – Current -AST 4 sample 3 high voltage steps

4. Preliminary simulations results

Accelerated stress tests 1, 3 and 4 were then simulated with the model. The particle radius distribution was represented with a log normal distribution, discretized in 16 particle groups, which reproduces the real initial distribution, determined with a TEM-based analysis made at CEA-Grenoble institute.

With the parameters previously calibrated on experimental data (SET 0), the model was not able to reproduce experimental results. Indeed, the PtO is completely reduced at 0.7 V (Figure 12). This results in similar oxide profiles for the different ASTs voltage profiles, and consequently in similar anodic dissolution rate and ECSA loss. Moreover, this behavior is not in agreement with experimental results, which suggests that the oxide is completely reduced only at lower potential values (< 0.4 V).

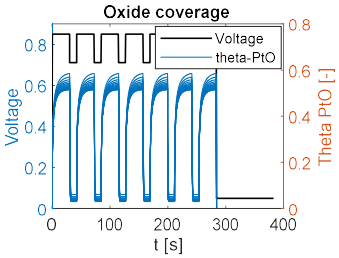

Figure 12 - AST 1 sample 1 base cycle oxide profile – SET 0

Parameters were then varied aiming to reproduce the expected oxide profiles and the experimental ECSA trends. The oxidation equilibrium potential Φ_{ox}^{ref} and the kinetic constant k_{ox} were reduced to move the oxide reduction towards lower potentials, thus obtaining different oxide profiles for different voltage profiles, as shown in Figure 13. The anodic dissolution kinetic constant k_{dis}^{ref} was then slightly increased to enhance degradation. AST 3 was simulated with these parameters (SET 1). The obtained ECSA trends are quite close to

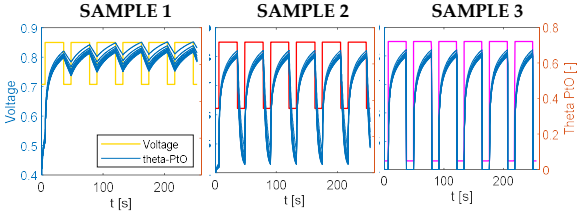

Figure 13 - AST 3 oxide profiles (parameter SET 1)

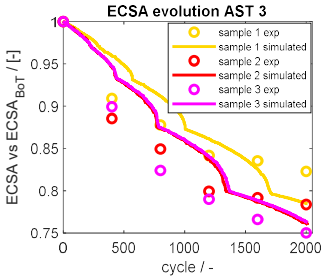

Figure 14 – ECSA trend: AST 3 - SET 1

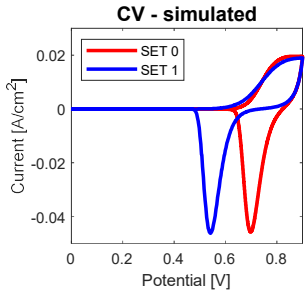

Figure 15– CV- SR 0.1 V/s - simulated with different parameters SETS

experimental results (Figure 14), but sample 2 and 3 are overlapped.

Moreover, CVs simulated with these parameters (Figure15) provide a worse approximation of the experimental one. The oxide reduction peak is indeed shifted toward lower potential values, lower than the one usually considered in the literature for PtO reduction [2][7].

In conclusion, the model is not able to reproduce the experimental data, even by changing the parameters set. This suggests the need for a further development of the model, also including more complex oxidation and dissolution mechanisms.

5. Model: a further development

A more complex model has been implemented, adding two reactions, namely place exchange and cathodic dissolution (reactions (7) and (9)), described in the following.

$$PtO \rightleftarrows OPt \quad (7)$$

$$OPt \rightarrow PtO_2 \quad (8)$$

$$PtO_2 + 2e^- + 4H^+ \rightarrow 2H_2O + Pt^{2+} \quad (9)$$

When the potential reaches high values, or a certain potential is kept constant long enough, the O atoms can undergo a place exchange from surface to subsurface position [8], exposing Pt atoms once again so that the oxides begin to build deeper into the platinum lattice. It is not clear whether the driving force of this mechanisms is the potential or the oxide coverage, as both conditions occur simultaneously. At high potentials oxidation is enhanced, so that place-exchanged atoms are rapidly oxidized to PtO_2 (reaction (8)). Although the PtO_2 oxide coverage is not calculated in the model, it can be considered equivalent the OPt oxide coverage, as the oxidation reaction is really fast (at high potential) and irreversible. While in deaerated solutions the place exchange is usually considered relevant above 1.15 V, different values, as low as 0.75 V [9], have been reported in the presence of oxygen. When the potential decreases, an oxide reduction and an increase of Pt concentration is experimentally observed [10]. This is ascribed to a direct dissolution of place-exchanged oxides in the electrolyte, the so-called cathodic dissolution (reaction (9)).

Place exchange and cathodic dissolution can explain some of the experimental results. The current trends can be explained with the formation of two oxides: a simple one (PtO), reduced at higher potential values, and a more resistant one (OPt), which is not completely reduced even for values as low as 0.4 V.

This perspective also justifies the strong degrading effect of the short stops, as well as the increasing degradation observed in AST 3 and 4 for samples reaching lower potential values. The resistant oxide is accumulated when the cell voltage is kept above 0.7 V and dissolved when going to lower potential values. For lower potential values a stronger dissolution takes place, cleaning the catalyst active area from oxides but also causing a stronger degradation.

Place exchange is modelled as a reversible chemical reaction, not directly dependent on potential. The reaction rate expression (equation (10)) is taken from Karan [11], while the cathodic dissolution reaction rate (equation (11)) is adapted from Jahnke dissolution model [3].

$$r_{PE} = k_{PE}\vartheta_{PtO}(1-\vartheta_{OPt})\exp\left(-\omega_{PE} * \frac{\vartheta_{OPt}}{RT}\right) - k_{PE,r}\vartheta_{OPt} \quad (10)$$

$$r_{Cdiss}(r) = k_{Cdiss}\,\theta_{OPt}\exp\left(-\frac{\alpha_3 F}{RT}(\Phi - \Phi_{Cd})\right) \quad (11)$$

The idea behind this semi-empirical modelling of cathodic dissolution is that place-exchanged Pt-atoms can be considered as oxidized. During decreasing potential sweeps the oxide is reduced, and the place-exchanged oxide dissolve directly in the electrolyte according to cathodic dissolution, which in this sense can be considered potential-dependent.

Anodic dissolution and oxidation reaction rates remain unchanged in the model, while the chemical dissolution is replaced by the cathodic dissolution. Finally, material balances are corrected including the new reactions rates, and a new balance for the OPt oxide coverage is added.

At first, place exchange and cathodic dissolution parameters were taken from the literature [11][3]. Then the model was calibrated on the experimental

results of AST 4: they provide data for different potential profiles, and the cathodic dissolution is expected to be a prevailing mechanism in this AST, as previously explained.

A sensitivity analysis was performed varying α_3 and the kinetic constant k_{Cdiss}. For increasing values of α_3, the effect of different potential profiles is strengthened, resulting in more distant ECSA trends for samples reaching different minimum potential values. For increasing value of k_{Cdiss} a higher degradation is obtained. This effect is more marked for samples with lower minimum potential, where cathodic dissolution is indeed supposed to be more significant. Moreover, the kinetic constant of the backward place exchange $k_{PE,r}$ was decreased to obtain an increasing OPt profile during the AST cycle, as suggested by the experimental observations. Anodic dissolution and oxidation parameters were set again to the values obtained from calibration (SET 0).

The base profile of AST 4 sample 4 obtained with the final parameters set, which will be referred to as SET 4, is shown in Figure 16. OPt gradually increases during the AST cycle and is significantly reduced only going to 0.2 V, while the PtO (not shown) is almost totally reduced at 0.7 V. The cathodic dissolution reaction rate assumes low values during the cycling, with a peak during the final holding, which is more pronounced for sample 4, gradually less marked for samples 3 and 2, and absent for sample 1. These features are in agreement with the experimental results analysis.

The parameters effect was preliminarily evaluated by looking at the platinum dissolved in one AST cycle, analysing the different contribution given by the anodic dissolution, the cathodic dissolution during the cycling, and the cathodic dissolution during the final holding. These quantities are shown in Figure 17 for the four samples, identified by the final holding potential. Anodic dissolution has the same impact on the different samples, as it depends on the PtO profile, which is equal for the different samples. Cathodic dissolution has the same impact during the cycling, and an increasing impact during the final holding for samples with a lower holding potential.

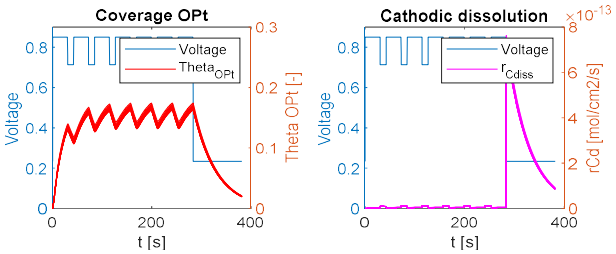

Figure 16 - OPt profile and cathodic dissolution: AST 4 sample 4 – parameters SET 4

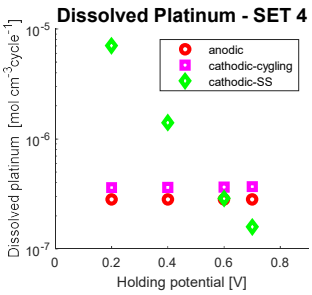

Figure 17- Pt dissolved in AST4 base cycle

AST 4 simulated ECSA trends are shown in Figure 18. AST 1 and AST 3 were also simulated with these parameters, and the resulting ECSA trends are shown in Figure 19.

AST 3 and AST 4 simulated ECSA trends show a good agreement with experimental results. This improved correspondence with experimental data suggests that cathodic dissolution have a prevailing effect in realistic degradation, which is reproduced with ASTs. Nonetheless, the improvement in the model does not allow to exactly reproduce the actual effect of potential. Indeed, the potential value weakly affects the results in the range between 0.85 V and 0.6 V (resulting in similar degradation for samples 1 and 2 of AST 3 and sample 1 and 2 of AST 4 respectively), while it has a gradually stronger impact going toward lower values. Approaching 0 V the potential effect is too strong with respect to experimental results of AST 1.

Moreover, the simulated trends are characterized by an almost linear evolution, and stabilize only when a really strong degradation takes place (i.e. in AST 1 simulation), while experimental results show a stabilization also for limited ECSA loss.

The model could be further improved by stressing the effect of particle size on the degradation with the

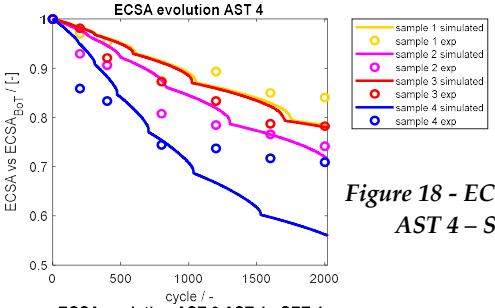

Figure 18 - ECSA trend: AST 4 – SET 4

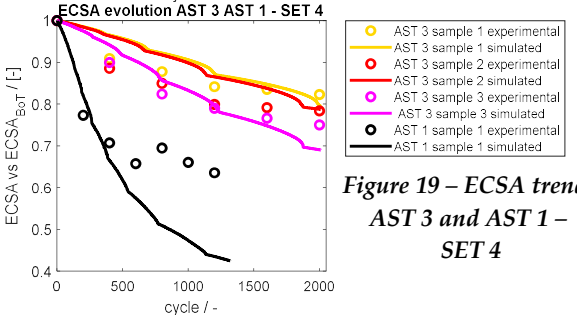

Figure 19 – ECSA trend: AST 3 and AST 1 – SET 4

introduction of a dependence of the cathodic dissolution on the particle radius. Indeed, it could be reasonably assumed that size and geometry of the particles impact on the dissolution rate, making larger particles less prone. This would result in a faster initial degradation due to the strong dissolution of smaller particles and a progressive stabilization when the PRD is shifted toward higher radius.

6. Conclusions

A 0-D model was developed to simulate platinum dissolution in normal low power operating conditions, given different voltage profiles. The model in its first version includes only one oxide and one dissolution reaction (anodic dissolution). Parameters were calibrated on experimental data.

An experimental analysis was performed by means of several ASTs with different potential profiles, starting from the IDFAST Low Power AST. The experimental results show that cycling above 0.7 V has a low degrading effect, regardless of the UPL, differently from the general knowledge available in the literature. A stronger degradation is obtained by decreasing the minimum potential, both when it is continuously reduced under 0.7 V, and when it is only periodically reduced under this value. Currents trends suggest the presence of an oxide which is not reduced at 0.7 V but only going at lower potential values (< 0.4 V).

The model in its first version was not able to reproduce experimental results. It was thus developed adding place exchange mechanism and cathodic dissolution, which could provide a better explanation of experimental results. The role of these reactions is still not fully clarified in the literature. With the aid of a sensitivity analysis the parameters were calibrated on experimental data, obtaining a better correspondence. This suggests that cathodic dissolution have a prevailing effect in realistic operation, characterized by long holding times in hydrogen/air, which was reproduced with ASTs. The model resulted as a useful tool for interpreting the main drivers of catalyst layer ageing. It can be further improved and calibrated to reproduce more accurately the effect of potential limits on degradation and the stabilization of ECSA trend. In particular, it could be used for better describing the stop process at low potential values, in order to limit the dissolution caused by such operation, the relevant role of which was highlighted by the experimental campaign.

References

[1] A. Kneer and N. Wagner, "A Semi-Empirical Catalyst Degradation Model Based on Voltage Cycling under Automotive Operating Conditions in PEM Fuel Cells," *J. Electrochem. Soc.*, vol. 166, no. 2, pp. F120–F127, 2019.

[2] P. Schneider, C. Sadeler, A.-C. Scherzer, N. Zamel, and D. Gerteisen, "Fast and Reliable State-of-Health Model of a PEM Cathode Catalyst Layer," *J. Electrochem. Soc.*, vol. 166, no. 4, pp. F322–F333, 2019.

[3] T. Jahnke, A. Baricci, C. Rabissi, and A. Casalegno, " Erratum: Physical Modeling of Catalyst Degradation in Low Temperature Fuel Cells: Platinum Oxidation, Dissolution, Particle Growth and Platinum Band Formation [J. Electrochem. Soc. , 167 , 013523 (2020)] ," *J. Electrochem. Soc.*, vol. 167, no. 14, p. 149001, 2020.

[4] D. Mora, "Design and validation of new Accelerated Stress Tests for the experimental analysis of hydrogen PEM fuel cell degradation under real world automotive operation," 2022.

[5] T. F. Cells, F. Cell, T. Office, F. Cells, T. Office, and T. F. Cells, "3.4 Fuel Cells," vol. 2015, pp. 1–58, 2016.

[6] "index @ www.id-fast.eu." .

[7] H. A. Baroody, E. Kjeang, J. E. Soc, H. A. Baroody, and E. Kjeang, "Predicting Platinum Dissolution and Performance Degradation under Drive Cycle Operation of Polymer Electrolyte Fuel Cells Predicting Platinum Dissolution and Performance Degradation under Drive Cycle Operation of Polymer Electrolyte Fuel Cells," 2021.

[8] A. A. Topalov, S. Cherevko, A. R. Zeradjanin, J. C. Meier, I. Katsounaros, and K. J. J. Mayrhofer, "Towards a comprehensive understanding of platinum dissolution in acidic media," *Chem. Sci.*, vol. 5, no. 2, pp. 631–638, 2014.

[9] A. Kongkanand and J. M. Ziegelbauer, "Surface Platinum Electrooxidation in the Presence of Oxygen," 2012.

[10] R. K. Ahluwalia *et al.*, "Potential Dependence of Pt and Co Dissolution from Platinum-Cobalt Alloy PEFC Catalysts Using Time-Resolved Measurements JES F OCUS I SSUE ON P ROTON E XCHANGE M EMBRANE F UEL C ELL (PEMFC) D URABILITY Potential Dependence of Pt and Co Dissolution from ," 2018.

[11] B. Jayasankar and K. Karan, "O2 electrochemistry on Pt: A unified multi-step model for oxygen reduction and oxide growth," *Electrochim. Acta*, vol. 273, pp. 367–378, 2018.

Acknowledgements

This work has been developed in the framework of the European ID-FAST project, which has received funding from the Fuel Cells and Hydrogen 2 Joint Undertaking under the European Union's Horizon 2020 research and innovation program (grant agreement No. 779565).